Geophysical Research Letters

RESEARCH LETTER
10.1029/2023GL105448

Surface Ocean Cooling in the Eocene North Atlantic Coincides With Declining Atmospheric CO_2

Gordon N. Inglis[1], Rehemat Bhatia[2], David Evans[1,3], Jiang Zhu[4], Wolfgang Müller[3], David Mattey[5], David J. R. Thornalley[6], Richard G. Stockey[1], and Bridget S. Wade[2]

[1]School of Ocean and Earth Science, University of Southampton, Southampton, UK, [2]Department of Earth Sciences, University College London, London, UK, [3]Institute of Geosciences, Goethe University Frankfurt, Frankfurt, Germany, [4]National Center for Atmospheric Research, Boulder, CO, USA, [5]Department of Earth Sciences, Royal Holloway University of London (RHUL), Egham, UK, [6]Department of Geography, University College London, London, UK

Gordon N. Inglis and Rehemat Bhatia contributed equally to this work.

Key Points:

- Long-term (~4°C) decline in North Atlantic sea surface temperatures (SSTs) between the early (~53–49 Ma) and middle (~44–41 Ma) Eocene
- This indicates that CO_2 was likely responsible for the onset of long-term Eocene cooling
- However, east-west temperature gradients in the North Atlantic are decoupled, possibly due to additional non-CO_2 forcing mechanisms

Supporting Information:

Supporting Information may be found in the online version of this article.

Correspondence to:

G. N. Inglis and R. Bhatia,
gordon.inglis@soton.ac.uk;
rehemat.bhatia.13@alumni.ucl.ac.uk

Citation:

Inglis, G. N., Bhatia, R., Evans, D., Zhu, J., Müller, W., Mattey, D., et al. (2023). Surface ocean cooling in the Eocene North Atlantic coincides with declining atmospheric CO_2. *Geophysical Research Letters*, *50*, e2023GL105448. https://doi.org/10.1029/2023GL105448

Received 24 JUL 2023
Accepted 29 NOV 2023

Author Contributions:

Conceptualization: Gordon N. Inglis, Rehemat Bhatia, Bridget S. Wade
Data curation: Gordon N. Inglis, Rehemat Bhatia
Formal analysis: David Evans, Jiang Zhu, Richard G. Stockey
Funding acquisition: Gordon N. Inglis, Rehemat Bhatia, Bridget S. Wade
Investigation: Gordon N. Inglis, Richard G. Stockey, Bridget S. Wade

Abstract The Eocene (56–34 million years ago) is characterized by declining sea surface temperatures (SSTs) in the low latitudes (~4°C) and high southern latitudes (~8–11°C), in accord with decreasing CO_2 estimates. However, in the mid-to-high northern latitudes there is no evidence for surface water cooling, suggesting thermal decoupling between northern and southern hemispheres and additional non-CO_2 controls. To explore this further, we present a multi-proxy (Mg/Ca, $\delta^{18}O$, TEX_{86}) SST record from Bass River in the western North Atlantic. Our compiled multi-proxy SST record confirms a net decline in SSTs (~4°C) between the early Eocene Climatic Optimum (53.3–49.1 Ma) and mid-Eocene (~44–41 Ma), supporting declining atmospheric CO_2 as the primary mechanism of Eocene cooling. However, from the mid-Eocene onwards, east-west North Atlantic temperature gradients exhibit different trends, which we attribute to incursion of warmer waters into the eastern North Atlantic and inception of Northern Component Water across the early-middle Eocene transition.

Plain Language Summary Over the past 541 million years, the Earth has oscillated between warm (greenhouse) and cold (icehouse) climates. The most recent transition between a greenhouse and icehouse climate state occurred during the Eocene (56–34 million years ago). This transition shows a gradual cooling, previously suggested to be driven by a decline in atmospheric carbon dioxide (CO_2). However, we know little about this transition in the North Atlantic Ocean. Previous studies show limited cooling of surface waters in this region. This suggests that changes in North Atlantic temperatures are not driven by CO_2. To understand how sea surface temperature changes in the western North Atlantic, we analyzed the chemistry of microscopic marine fossils in sediments. Our results show a 4°C decline in temperature from the early (~53 Ma) to the middle Eocene (~42 Ma). This matches computer simulations of Eocene climate and confirms CO_2 was responsible for the transition. The lack of cooling observed in previous work is probably due to the development of an ancient water mass known as Northern Component Water (observed today as North Atlantic Deep Water) and changes in how the Eocene ocean transported heat.

1. Introduction

The early Eocene Climatic Optimum (EECO; 53.3 to 49.1 million years ago; Ma) (Hollis et al., 2019; Zachos et al., 2001) is characterized by a long-term maximum in atmospheric CO_2 (~1,470 ppm) (Anagnostou et al., 2020), followed by a gradual decline in atmospheric CO_2 during the middle Eocene (47.8–38.0 Ma) to ~800 ppm (Anagnostou et al., 2020). This is consistent with declining SSTs in the tropics (ca. 4°C) (Cramwinckel et al., 2018; Evans et al., 2018) and the mid-to-high southern latitudes (ca. 8–11 °C; Bijl et al., 2009; Hollis et al., 2009, 2012). However, SST estimates from the eastern North Atlantic suggest relatively muted surface water cooling (~1°C) between the EECO and middle Eocene (~40 Ma) (Bornemann et al., 2016). Temperature asymmetry between the northern and southern hemisphere would not be expected from a long-term decline in atmospheric CO_2 alone (Liu et al., 2018) and suggests that other non-CO_2 driving mechanisms (e.g., gateway reorganization and/or changes in ocean circulation) may influence regional SST patterns.

Of particular relevance is the growing evidence for Northern Component Water (NCW) initiation in the North Atlantic during the early-middle Eocene (~49 and 47 Ma) (Boyle et al., 2017; Hohbein et al., 2012; Norris et al., 2001). The onset of NCW has been attributed to gateway reorganisation, specifically deepening of the

Methodology: Gordon N. Inglis, Rehemat Bhatia, David Evans, Wolfgang Müller, David Mattey
Project Administration: Gordon N. Inglis, Rehemat Bhatia
Software: Jiang Zhu, Richard G. Stockey
Supervision: David J. R. Thornalley, Bridget S. Wade
Visualization: Gordon N. Inglis, Rehemat Bhatia
Writing – original draft: Gordon N. Inglis, Rehemat Bhatia, David Evans, Bridget S. Wade
Writing – review & editing: Gordon N. Inglis, Rehemat Bhatia, David Evans, Jiang Zhu, Wolfgang Müller, David Mattey, David J. R. Thornalley, Richard G. Stockey, Bridget S. Wade

Greenland-Scotland Ridge (GSR) (Boyle et al., 2017; Hohbein et al., 2012; Vahlenkamp et al., 2018), although other mechanisms have been proposed such as isolation of the Arctic Ocean (Z. Zhang et al., 2011) or restriction of the Tethys Ocean (Roberts et al., 2009). The onset of NCW is followed by a period of weaker overturning (~42–38 Ma) (Witkowski et al., 2021), before re-invigoration of NCW during the late Eocene (~38 Ma) (Coxall et al., 2018) or Eocene-Oligocene transition (EOT; ~34 Ma) (Hutchinson et al., 2019). The establishment of NCW can transport additional heat into the eastern North Atlantic (Vahlenkamp et al., 2018), potentially muting any long-term cooling trend in this region and has been invoked to explain stable temperatures in the eastern North Atlantic during the middle Eocene (Bornemann et al., 2016). However, our understanding of long-term North Atlantic temperature change is based on a single proxy record (planktonic foraminiferal $\delta^{18}O$) from a single site (DSDP Site 401; Bornemann et al., 2016) and may not be regionally representative.

To test whether the wider North Atlantic region exhibits stable temperatures during the Eocene, we use a multi-proxy approach ($\delta^{18}O$, Mg/Ca, TEX_{86}) to reconstruct SST in the western North Atlantic (Bass River; ODP Leg 174AX; ~36°N paleolatitude) during the early-to-middle Eocene (53.7–42.0 Ma). We compare our new data set with climate model simulations spanning a wide range of CO_2 values to explore (a) temporal and spatial patterns of cooling in the North Atlantic during the Eocene and (b) whether there is thermal decoupling between the northern and southern hemisphere during the Eocene. This allows us to test whether declining CO_2 is the primary driver of long-term Eocene cooling or whether regional forcing mechanisms are also important.

2. Methods

2.1. Site Description

The Bass River section (ODP Leg 174AX; 39°36'N, 74°26'W) consists of calcareous marls and glauconitic silty clays deposited in middle to outer neritic paleodepths between 30 and 150 m (Fung et al., 2019; Miller et al., 1998, 2003). The biostratigraphic age model was developed using planktonic foraminifera and nannofossils (following Fung et al., 2019) with datums converted to the GTS2012 (Vandenberghe et al., 2012). Sediments span the early to middle Eocene (53.7–42.0 Ma) and encompass the EECO (~340–291 m). However, there are a series of hiatuses between ~49 and 44 Ma.

2.2. Analytical Methods

Lipid biomarker analysis was performed on 47 sediment samples. Approximately 5–10 g of sediment was extracted with an Ethos Ex microwave extraction system using 15 ml of dichloromethane (DCM) and methanol (MeOH) (9:1, *v/v*). The total lipid extract was separated over silica into apolar and polar fractions using hexane:dichloromethane (9:1, *v/v*) and dichloromethane:methanol (1:2, *v/v*), respectively. The polar fraction (containing isoGDGTs) was dissolved in hexane:isopropanol (99:1, *v/v*), passed through 0.45 µm PTFE filters and analyzed by HPLC/APCI-MS following Hopmans et al. (2016). Trace element and stable oxygen isotope ($\delta^{18}O$) planktonic foraminiferal analysis was performed on multiple depth intervals ($n = 8$) spanning the early-to-middle Eocene. Foraminiferal preservation is excellent, appearing transparent or translucent under the light microscope, with no signs of diagenetic alteration observed under SEM (Figure S1 and Table S1 in Supporting Information S1). Analysis was performed on various surface-dwelling species (*Acarinina praetopilensis*, *Morozovella formosa*, *Morozovelloides crassatus*, and *Pseudohastigerina wilcoxensis*) and deeper, thermocline-dwelling species (*Parasubbotina hagni*, *Parasubbotina inaequispira*). Single-specimen Mg/Ca analysis was performed via slow depth-profiling by laser ablation-inductively coupled plasma mass spectrometry (LA-ICPMS) (see Müller et al., 2009; Table S2 in Supporting Information S1). Mg/Ca values were determined in multiple chambers (~3–5) within a single specimen and averaged. The same specimens were subsequently analyzed for $\delta^{18}O$ using a Multiprep-Isoprime 100 dual inlet system optimized for analysis of single specimens (Supporting Information S1).

2.3. Temperature Calibrations

TEX_{86} data was screened using established indices for non-Thaumarchaeota inputs (Figure S5 in Supporting Information S1) and converted to SST using a Bayesian linear calibration (prior mean = 25, prior standard deviation = 10, $n = 2{,}000$) (Tierney & Tingley, 2014). Planktonic foraminiferal $\delta^{18}O$ values were converted to SST using the bayfox Bayesian calibration (prior mean = 25, prior standard deviation = 20, $n = 2{,}000$). Seawater

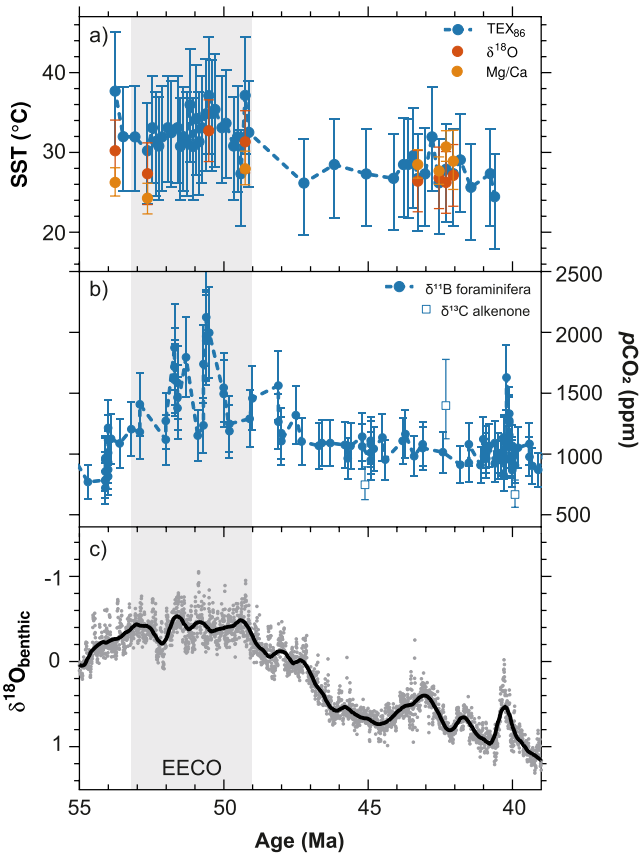

Figure 1. (a) SST reconstructions from Bass River during the early-middle Eocene inferred via TEX_{86} (blue), planktonic foraminifera $\delta^{18}O$ (dark orange) and Mg/Ca (light orange). Error bars represent the 95% confidence intervals. (b) Atmospheric CO_2 reconstructions inferred via planktonic foraminifera $\delta^{11}B$ (blue circles) and alkenone $\delta^{13}C$ (blue squares). Error bars represent ±1 standard deviation (Rae et al., 2021). (c) benthic foraminifera $\delta^{18}O$ values (Westerhold et al., 2020).

$\delta^{18}O$ ($\delta^{18}O_{sw}$) values were obtained via the isotope-enabled Community Earth System Model version 1.2 (iCESM1.2; see below). Mg/Ca values were converted into SST using a modified version of MgCaRB (Gray and Evans, 2019) (Supporting Information S1). We report pH-corrected Mg/Ca temperatures as the majority of modern foraminifer species are characterized by Mg/Ca-pH sensitivity (Gray and Evans, 2019). Planktonic foraminifera were rare and thus for Mg/Ca and $\delta^{18}O$, we report the "average" SST estimates for a given time slice ($n = 8$ for $\delta^{18}O$, $n = 7$ for Mg/Ca) by combining (a) multiple-specimens from multiple size fractions and (b) all surface-dwelling species within multiple genera (i.e., *Acarinina praetopilensis*, *Acarinina pseudotopilensis*, *Morozovella formosa*, *Morozovelloides crassatus*, *Pseudohastigerina wilcoxensis*) into a single estimate, following DeepMIP protocols (Hollis et al., 2019; Supporting Information S1). Average "SST" estimates comprise a minimum of two samples from a single depth horizon (see Data S4 and S5 in Supporting Information S1). When SSTs are calculated using individual species (Figure S2 in Supporting Information S1) and size segregating species (Figures S2 and S3 in Supporting Information S1), similar patterns in long-term trends are observed.

2.4. Climate Model Simulations

We use the water isotope-enabled Community Earth System Model version 1.2 (iCESM1.2) (Zhu et al., 2019, 2020) to compare with our proxy reconstruction and to provide an independent estimate of $\delta^{18}O_{sw}$. iCESM1.2 is able to closely replicate large-scale features of early Eocene climate, including: (a) enhanced global mean surface temperature estimates (Lunt et al., 2021; Zhu et al., 2019), (b) reduced meridional temperature gradients (Lunt et al., 2021), (c) changes in the hydrological cycle (Cramwinckel et al., 2023), and (d) the values and distribution of planktonic foraminifera $\delta^{18}O$ values (Zhu et al., 2020). It is also the only DeepMIP model that has water isotopes enabled (Zhu et al., 2020). The iCESM1.2 simulations were performed following the Deep-time Model Intercomparison Project protocols (Lunt et al., 2017) with early Eocene paleogeography and vegetation (56.0–47.8 Ma) (Herold et al., 2014) and atmospheric CO_2 levels of 1×, 3×, 6×, and 9× preindustrial values (284.7 ppmv). Seawater $\delta^{18}O$ in the simulations was initialized from a constant value of −1.0‰ to account for the absence of ice sheets in a hothouse climate (Hollis et al., 2019; Shackleton & Kennett, 1975). Previous studies at Bass River have suggested sea level changes through the middle Eocene on the order of 20–30 m, that have been attributed to changes in Antarctic ice volume (Fung et al., 2019). We do not adjust $\delta^{18}O_{sw}$ in this study for middle Eocene ice volume fluctuations, as the timing and magnitude of these ephemeral glaciations are currently poorly constrained and our planktonic $\delta^{18}O$ data from Bass River are from intervals where water depth was greatest (i.e., ice volume was minimal). Our model results indicate only minor changes in $\delta^{18}O_{sw}$ at the Bass River location through the early-middle Eocene (~0.2‰ change between 1× and 9× CO_2 simulations using iCESM1.2; Table S3 in Supporting Information S1). As such, we use the average $\delta^{18}O_{sw}$ value (−0.54‰) to calculate planktonic foraminiferal $\delta^{18}O$-derived SST estimates. See Zhu et al. (2019, 2020) and Y. Zhang et al. (2022) for further details of the experimental setup and equilibration state.

3. Results

During the EECO (53.3–49.1 Ma), TEX_{86} SST estimates average ~33°C (Figure 1a). Between the EECO and the middle Eocene (44–41 Ma), TEX_{86} SST estimates decline by ~5°C (Figure 1a). Oxygen isotope SST estimates during the EECO from surface-dwelling planktonic foraminifera average ~32°C (Figure 1a). Surface-dwelling species yield higher temperatures (up to ~5°C higher) than thermocline-dwelling species but exhibit a similar magnitude of cooling (~4°C) between the EECO and the middle Eocene (44–41 Ma). During the early Eocene, Mg/Ca SST estimates (calculated using the *G. ruber* calibration) average ~27°C (Figure 1a). These values are

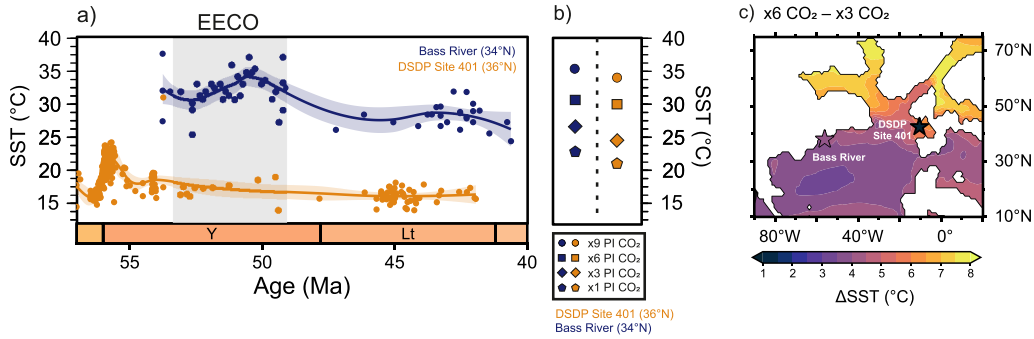

Figure 2. Divergent zonal temperature gradients in the North Atlantic during the early-to-middle Eocene. (a) proxy-derived sea surface temperature (SST) reconstructions for Bass River (*this study;* blue symbols) and DSDP Site 401 ($\delta^{18}O$ only; orange symbols) (Bornemann et al., 2016) fitted with a LOESS regression. $\delta^{18}O$ values from DSDP Site 401 re-calculated for surface-dwelling foraminiferal genera (*Acarinina and Morozovella* spp.) using the bayfox Bayesian calibration ($\delta^{18}O_{sw} = -0.81$, prior mean = 25, prior standard deviation = 20, $n = 2{,}000$). $\delta^{18}O_{sw}$ values obtained via iCESM1.2 (Table S3 in Supporting Information S1). Error bars represent the 95% confidence intervals. (b) iCESM1.2-derived SST estimates for Bass River (blue symbols) and DSDP Site 401 (orange symbols) under different CO_2 concentrations, (c) iCESM1.2-derived ΔSST estimates (x6 PI CO_2 - x3 PI CO_2) with proxy-derived cooling between the early- to middle Eocene shown for each site.

lower than $\delta^{18}O$ and TEX_{86} SST estimates by ~5°C and ~6°C, respectively; Figure 1a but agree within the propagated calibration uncertainties. Mg/Ca SST estimates increase by ~3°C between the EECO and middle Eocene (44–41 Ma; Figure 1a). However, the absolute values (~30°C) are comparable to middle Eocene-aged TEX_{86} and $\delta^{18}O$ SST estimates (28°C and 29°C, respectively) and agree within the propagated calibration uncertainties.

4. Discussion

4.1. Long-Term Cooling in the Western North Atlantic During the Eocene

The use of multiple proxies provides more robust long-term temperature records than a single proxy. The consistency between Mg/Ca, oxygen isotopes and TEX_{86} values in the EECO and late Eocene is encouraging and indicates that each proxy is recording the same environmental signal (i.e., SST). TEX_{86} and $\delta^{18}O$ values indicate very high SSTs at Bass River during the EECO (~32–33°C). These values are in agreement with existing low-resolution TEX_{86} estimates generated at Bass River (de Bar et al., 2019) and nearby South Dover Bridge (~34°C; Inglis et al., 2015). Mg/Ca SST estimated are also relatively high (~27°C; Figure 1) but are lower than TEX_{86} and $\delta^{18}O$-derived SST estimates by ~5–6°C. Between the EECO and middle Eocene (44–41 Ma), TEX_{86} and $\delta^{18}O$ values indicate gradual surface water cooling (5 and 4°C, respectively; Figure 1a), coherent with declining TEX_{86} SSTs (~7°C) at South Dover Bridge between the EECO and middle Eocene (~42 Ma). Evidence of cooling in two independent proxies (TEX_{86}, $\delta^{18}O$) and locations provides the first compelling evidence for surface ocean cooling in the (western) North Atlantic between the early and middle Eocene, which is in parallel with the inferred deep-ocean cooling in benthic foraminifera $\delta^{18}O$ record (Figure 1b; Westerhold et al., 2020).

In contrast, our new Mg/Ca SSTs increase by ~3°C between the EECO and middle Eocene. Although middle Eocene (44–41 Ma) SST estimates are in excellent agreement with TEX_{86} and $\delta^{18}O$ values (Figure 1) and alkenone-derived SST estimates (~29–30°C; Liu et al., 2018) from nearby site IODP Site 1404, the temporal trends are inconsistent with regional observations (*this paper*) (de Bar et al., 2019; Inglis et al., 2015) and declining global bottom water temperature estimates inferred via changes in benthic foraminiferal $\delta^{18}O$ values (Figure 1b) (Westerhold et al., 2020). To explore this mismatch further, we compared our proxy-derived temperature estimates (TEX_{86}, Mg/Ca, $\delta^{18}O$) from the EECO (53.3–49.1 Ma; Hollis et al., 2019) and middle Eocene (44–41 Ma) alongside iCESM1.2 simulations with different CO_2 scenarios (1× to 9× pre-industrial CO_2) (Figure S6 in Supporting Information S1). These two intervals are chosen as they contain SST estimates from multiple proxies (Mg/Ca, $\delta^{18}O$, and TEX_{86}) and exhibit a similar sampling density. iCESM1.2 simulated SSTs at the Bass River are 31°C and 27°C in the 6× and 3× PI CO_2 simulations, respectively (Figure 2b), which overlaps with proxy reconstructions (Figure 2a; Figure S6 in Supporting Information S1). For a two-fold decrease in atmospheric CO_2 (i.e., from 6× to 3× PI CO_2), the model predicted decrease in SST of ~4°C is comparable to

the magnitude of cooling captured by TEX_{86} and $\delta^{18}O$ (5 and 4°C, respectively; Figure S6 in Supporting Information S1) between the EECO and middle Eocene, but is inconsistent with warming observed in Mg/Ca values. Given that proxy-derived CO_2 estimates decline from ~1,470 ppm (~5× PI CO_2) to ~800 ppm (~3× PI CO_2) during this interval (Anagnostou et al., 2020), this implies additional non-thermal controls on Mg/Ca values at this site.

The choice of Mg/Ca calibration remains uncertain when working with extinct species. However, the discrepancy between Mg/Ca-derived SSTs and other proxy data is insensitive to the choice of Mg/Ca calibration approach (Supporting Information S1). This is because seawater pH was substantially lower than modern throughout the Eocene (Anagnostou et al., 2020), such that choosing a *G. ruber* or *T. sacculifer*-like calibration has a minor effect on the long-term Mg/Ca-derived trend in our data set (Figure S3 in Supporting Information S1). Seawater Mg/Ca is also well-constrained for the Eocene (Evans et al., 2018; Gothmann et al., 2015) and is broadly invariant across this interval, such that it is very unlikely that unidentified changes mask cooling. Given that this site was targeted for its exceptional foraminiferal preservation and diverse assemblages (Figure S1 in Supporting Information S1), this potentially points toward either an evolutionary control on Eocene planktonic foraminifera Mg incorporation, or a shift in seawater carbonate chemistry at this site that substantially differs from the existing pH records (Anagnostou et al., 2020; Rae et al., 2021; see Supporting Information S1 for more discussion). Resolving this issue and exploring any other additional controls (e.g., local hydrographic variability; cf. Thornalley et al., 2011) will require further data and is beyond the scope of this study. We continue to include the Mg/Ca SST estimates in our assessment of the thermal evolution of Bass River (Figure 2a) and note that mismatches in $\delta^{18}O$ and Mg/Ca derived SSTs are not unique to deep-time species. Furthermore, this discrepancy in inorganic geochemical temperature reconstructions may ultimately stem from a small number of Mg/Ca analyses in the early Eocene, highlighting the benefit of working with a larger numbers of specimens, where possible.

4.2. Divergent Zonal Temperature Gradients in the North Atlantic During the Early-To-Middle Eocene

To determine the long-term mean SST evolution at Bass River, we fit LOESS regressions to our multi-proxy data set (TEX_{86}, Mg/Ca, $\delta^{18}O$) (Supporting Information S1). This approach indicates net cooling (~4°C) in the western North Atlantic between the EECO and middle Eocene (Figure 2a). Our data from the western North Atlantic contrasts with existing planktonic foraminifera $\delta^{18}O$-derived SST estimates from the eastern North Atlantic (~37°N; DSDP Site 401; Bornemann et al., 2016) that indicate minimal (<1°C) or no cooling between the EECO and late middle Eocene (ca. 42–40 Ma) (Figure 2a). CESM1.2 model simulations show that the magnitude of cooling at Bass River inferred via proxies is consistent with a halving of CO_2 (Figure 2c) but that the magnitude of proxy-inferred cooling at DSDP Site 401 is much lower than expected (Figures 2b and 2c). The east-west zonal mean temperature gradient inferred via proxy estimates (~15–20°C) is also larger than inferred via model simulations (~3°C; Figure 2b). As the model simulations are identical with the exception of changes in CO_2, this implies that non-CO_2 controls influence SSTs in the eastern North Atlantic (DSDP Site 401; Bornemann et al., 2016) during the Eocene.

Planktonic foraminifera at Bass River exhibit excellent preservation (Supporting Information S1) and tests are translucent and "glassy" (Figure S1 in Supporting Information S1) whereas Hollis et al. (2019) classified post-PETM planktonic foraminifera at DSDP Site 401 as "recrystallized." However, post-PETM foraminifera at DSDP Site 401 exhibit good preservation (Bornemann et al., 2016) and show limited evidence for recrystallization. If planktonic foraminifera had been subject to significant post-depositional alteration, they would be "reset" toward deep-sea temperatures and would track changes in benthic foraminiferal $\delta^{18}O$ values (Pearson et al., 2007). However, planktonic foraminiferal $\delta^{18}O$ values at DSDP Site 401 do not co-vary with benthic $\delta^{18}O$ values, either at this site (Bornemann et al., 2016) or elsewhere (Westerhold et al., 2020). Therefore, this is unlikely to explain the observed trends (Figure 2a). However, additional SST records from the North Atlantic are required to explore regional variations further.

Alternatively, changes in ocean circulation could have modulated regional temperature patterns in the eastern North Atlantic during the middle-to-late Eocene, specifically the onset of NCW formation. None of the DeepMIP models (including CESM1.2) show deep overturning circulation (>2,000 m) in the North Atlantic during the early Eocene (Y. Zhang et al., 2022), consistent with proxy evidence (e.g., benthic foraminifera $\delta^{13}C$ and fish teeth ε_{Nd} values; see Y. Zhang et al. (2022)). Instead, most of the DeepMIP models (and CESM simulations with 1× to 3× CO_2) suggests that deep water formation is likely to form in the Southern Ocean, which also broadly

agrees with proxy-based evidence from the early Eocene (Y. Zhang et al., 2022). CESM does simulate a North Atlantic deep/intermediate water formation at 1× PI CO_2, suggesting that NCW formation represents a delicate balance between multiple factors such as global or regional cooling, widening of the Atlantic basin, closure of the Arctic-Atlantic gateway (Hutchinson et al., 2019) and/or deepening/opening of the GSR (Straume et al., 2022; Vahlenkamp et al., 2018). The lack of deep water formation in iCESM1.2 at high CO_2 concentrations (i.e., 6× CO_2) is likely related to the initial condition and short integration length (see Y. Zhang et al., 2022 for further discussion). We speculate that this limitation in the iCESM1.2 simulation at 6× CO_2 would have a minor impact on the surface ocean of the North Atlantic, where regional ocean-atmosphere coupling and wind driven circulation are more important in determining the SSTs.

Idealized modeling experiments show that deepening of the GSR and/or closure of the Arctic-Atlantic gateway (Hutchinson et al., 2019) can initiate NCW formation in the North Atlantic and increase SST in the eastern North Atlantic by up to 7 °C (Vahlenkamp et al., 2018), thus muting any long-term CO_2-driven cooling at DSDP Site 401. Importantly, deepening of the GSR has only a minimal influence (<1°C) on SSTs in the western North Atlantic (i.e., where Bass River is located) (Vahlenkamp et al., 2018). There is growing geochemical and sedimentological evidence placing the initial onset of NCW between ~49 and 47 Ma, coincident with changes in zonal temperature gradients between the eastern and western North Atlantic. Evidence for onset of NCW between ~49 and 47 Ma includes development of contourite drifts in the western North Atlantic (Boyle et al., 2017), changes in biosiliceous sedimentation (Witkowski et al., 2021) and a collapse in $\delta^{13}C$ gradients between the North and South Atlantic (Hohbein et al., 2012). These changes would also influence local hydrography within the eastern North Atlantic and could exert an additional control on $\delta^{18}O_{sw}$ values at DSDP Site 401.

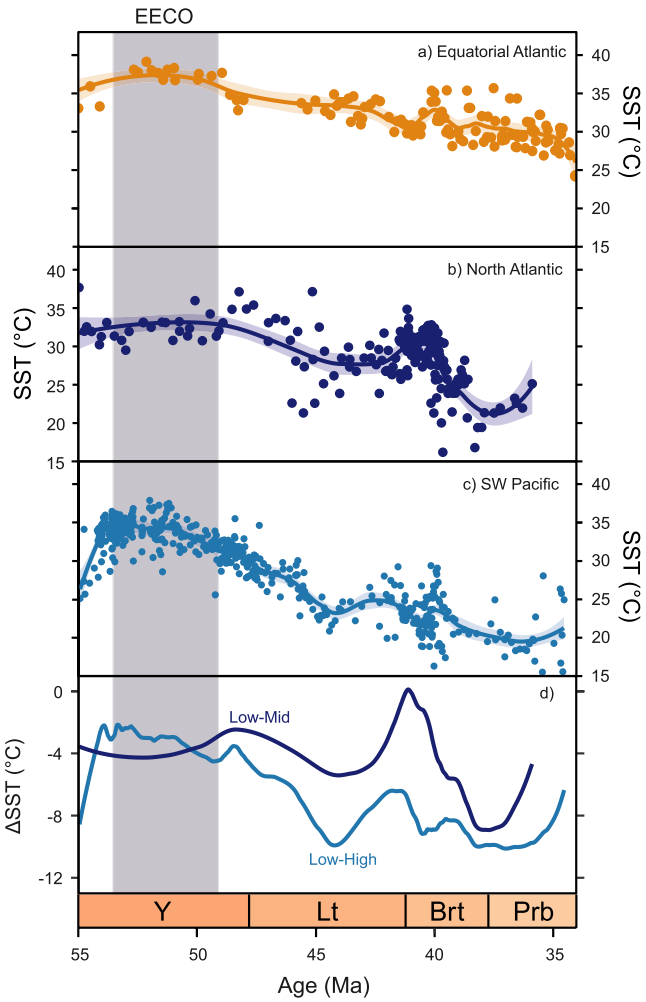

Figure 3. Long-term evolution of surface ocean temperatures during the Eocene inferred via TEX_{86} in the (a) equatorial Atlantic (Cramwinckel et al., 2018; Inglis et al., 2015; Zhang et al., 2013), (b) North Atlantic (this study; Inglis et al., 2015; de Bar et al., 2019), and (c) the southwest Pacific (Bijl et al., 2009, 2013; Crouch et al., 2020; Hollis et al., 2009; Inglis et al., 2015). Panel (d) shows the sea surface temperature (SST) gradient between the equatorial Atlantic and the North Atlantic (dark blue line) and southwest Pacific (light blue line). To determine the long-term mean SST evolution for the low-, mid-, and high-latitudes, nonparametric LOESS regressions were fitted using the fANCOVA software package (http://www.R-project.org/).

Proxy-based reconstructions during the Middle Eocene Climatic Optimum have argued that northward expansion of the North Atlantic subtropical gyre could also act as a mechanism to increase SSTs within the North Atlantic (Van Der Ploeg et al., 2023). However, details of the gyre heat transport and the impact of this large-scale process on regional SSTs (especially near coastlines) requires further investigation. Thus, although diverging zonal temperature gradients in the North Atlantic are consistent with the initial early onset of NCW during the early-middle Eocene, additional proxy data and isotope-enabled model simulations are required to test this further. From a model-based perspective, simulations with higher resolution and longer simulation length are required to explore the equilibrium state of the modeled ocean circulation and any possible regional features that may be missed by the relatively coarse (~1–2°) resolution model.

4.3. Synchronous Surface Water Cooling in the Northern and Southern Hemispheres During the Eocene

To explore whether long-term cooling is globally synchronous, we compiled TEX_{86}-derived SST estimates that span the early (55 Ma) to late (34 Ma) Eocene. To avoid relying on single proxy records, we focus on regions with two or more TEX_{86} records. Our data compilation spans three regions: (a) the equatorial Atlantic (0–30°N/S) (Cramwinckel et al., 2018; Inglis et al., 2015; Liu et al., 2009; Y. G. Zhang et al., 2013), (b) the northwest Atlantic (30–50°N) (*this study*; Cramwinckel, Coxall, et al., 2020; Inglis et al., 2015; Keating-Bitonti et al., 2011; van der Ploeg et al., 2023) and (c) the southwest Pacific (>50°S) (Bijl et al., 2009, 2013; Cramwinckel, Woelders, et al., 2020; Crouch et al., 2020; Hollis et al., 2009; Inglis et al., 2015; Liu et al., 2009) (Figure 3; Supporting Information S1).

Our results suggest that the onset of long-term cooling occurs ~49 to 48 million years ago in the North Atlantic and southwest Pacific (i.e., following the termination of the EECO; Figures 3a–3c) and coincides with an increase in the latitudinal SST gradient from 49 to 44 Ma (Figure 3d). Our study indicates that the onset of Eocene cooling is a global feature and thus consistent with a decline in atmospheric CO_2 as a forcing mechanism for cooling. However, there is a relative lack of data in the North Atlantic from ~49 to 48 Ma, such that additional records are required to determine the exact onset of long-term cooling. Proxy records have also suggested that ocean gateways may have played an important role at this time (e.g., Bijl et al., 2009, 2013; Hohbein et al., 2012). Previous work argues that the Tasman Gateway was open to shallow circulation at this time (~49–46 Ma) (Bijl et al., 2013). Deepening of the Tasman Gateway would initiate regional surface water cooling (Sijp et al., 2011, 2016) and may account for declining SSTs in the SW Pacific between the termination of the EECO and middle Eocene (~44 Ma). However, as surface ocean cooling occurs in multiple basins (Figures 3a–3c) at a comparable time (~49–48 Ma), it suggests that CO_2 was likely responsible for the majority of long-term Eocene cooling.

5. Conclusions

Here we present the first multi-proxy (Mg/Ca, $\delta^{18}O$, TEX_{86}) SST record from the western North Atlantic spanning the early-to-middle Eocene. Our results indicate very high SSTs during the early Eocene Climatic Optimum (~27–33°C), in agreement with high atmospheric CO_2 concentrations. Our compiled data set reveal a net decline (~4°C) in SSTs between the early Eocene Climatic Optimum (53.3–49.1 Ma) and the middle Eocene (44–41 Ma), consistent with long-term decrease in atmospheric CO_2. However, east-west zonal temperature gradients in the North Atlantic are likely decoupled during the early-to-middle Eocene. This may be related to inception of NCW at the early-middle Eocene transition and incursion of warmer waters into the eastern North Atlantic, but additional data sets are required to test this further. We also demonstrate that the onset of long-term Eocene cooling in the western North Atlantic (~49–48 Ma) occurs synchronously in other ocean basins (e.g., N. Atlantic vs. S. Pacific) and across different latitudinal bands, implying that CO_2 was likely responsible for the onset of long-term Eocene cooling.

Acknowledgments

Samples were provided by IODP which is sponsored by the NSF and participating countries. GNI was supported by a Royal Society Dorothy Hodgkin Fellowship (DHF\R1\191178) and NERC (NE/V018388/1). We thank NEIF-B for analytical support and Jim Davy for SEM imaging support. RB acknowledges funding from a NERC PhD studentship (no. 1352360), the Cushman Foundation for Foraminiferal Research (Joseph A. Cushman Award for Student Research), and a 2016 Geologists' Association New Researchers' Award. BW was supported by NERC (NE/V018361/1, NE/G014817). LA-ICPMS work at RHUL was partly funded by a 2014 NERC Capital Equipment Grant (CC073) to WM. The CESM project is supported primarily by the National Science Foundation (NSF). This material is based upon work supported by the National Center for Atmospheric Research, a major facility sponsored by the NSF under Cooperative Agreement No. 1852977. JZ was supported by NSF Grant 2202777. We thank Jim Browning for information on the age model and Tianchen He for support in trace element and isotope data interpretation. We thank David Hutchinson, Sarah Feakins and two anonymous reviewers whose thoughtful comments significantly improved the manuscript.

Data Availability Statement

Inorganic and organic geochemical data and associated sea surface temperature estimates are available at OSF (G. N. Inglis, 2023). The transformation of measured Mg/Ca into temperature was calculated using MgCaRB (Evans, 2023). Loess regressions were calculated using R (http://www.R-project.org).

References

Anagnostou, E., John, E. H., Babila, T., Sexton, P., Ridgwell, A., Lunt, D. J., et al. (2020). Proxy evidence for state-dependence of climate sensitivity in the Eocene greenhouse. *Nature Communications*, *11*(1), 1–9. https://doi.org/10.1038/s41467-020-17887-x

Bijl, P. K., Bendle, J. A. P., Bohaty, S. M., Pross, J., Schouten, S., Tauxe, L., et al. (2013). Eocene cooling linked to early flow across the Tasmanian Gateway. *Proceedings of the National Academy of Sciences*, *110*(24), 9645–9650. https://doi.org/10.1073/pnas.1220872110

Bijl, P. K., Schouten, S., Sluijs, A., Reichart, G.-J., Zachos, J. C., & Brinkhuis, H. (2009). Early Palaeogene temperature evolution of the southwest Pacific Ocean. *Nature*, *461*(7265), 776–779. https://doi.org/10.1038/nature08399

Bornemann, A., D'haenens, S., Norris, R. D., & Speijer, R. P. (2016). The demise of the early Eocene greenhouse—Decoupled deep and surface water cooling in the eastern North Atlantic. *Global and Planetary Change*, *145*, 130–140. https://doi.org/10.1016/j.gloplacha.2016.08.010

Boyle, P. R., Romans, B. W., Tucholke, B. E., Norris, R. D., Swift, S. A., & Sexton, P. F. (2017). Cenozoic North Atlantic deep circulation history recorded in contourite drifts, offshore Newfoundland, Canada. *Marine Geology*, *385*, 185–203. https://doi.org/10.1016/j.margeo.2016.12.014

Coxall, H. K., Huck, C. E., Huber, M., Lear, C. H., Legarda-Lisarri, A., O'regan, M., et al. (2018). Export of nutrient rich Northern component water preceded early Oligocene Antarctic glaciation. *Nature Geoscience*, *11*(3), 190–196. https://doi.org/10.1038/s41561-018-0069-9

Cramwinckel, M. J., Burls, N. J., Fahad, A. A., Knapp, S., West, C. K., Reichgelt, T., et al. (2023). Global and zonal-mean hydrological response to early Eocene warmth. *Paleoceanography and Paleoclimatology*, *38*(6), e2022PA004542. https://doi.org/10.1029/2022pa004542

Cramwinckel, M. J., Coxall, H. K., Śliwińska, K. K., Polling, M., Harper, D. T., Bijl, P. K., et al. (2020). A warm, stratified, and restricted Labrador Sea across the middle Eocene and its climatic optimum. *Paleoceanography and Paleoclimatology*, *35*(10), e2020PA003932. https://doi.org/10.1029/2020pa003932

Cramwinckel, M. J., Huber, M., Kocken, I. J., Agnini, C., Bijl, P. K., Bohaty, S. M., et al. (2018). Synchronous tropical and polar temperature evolution in the Eocene. *Nature*, *559*(7714), 382–386. https://doi.org/10.1038/s41586-018-0272-2

Cramwinckel, M. J., Woelders, L., Huurdeman, E. P., Peterse, F., Gallagher, S. J., Pross, J., et al. (2020). Surface-circulation change in the southwest Pacific Ocean across the middle Eocene climatic Optimum: Inferences from dinoflagellate cysts and biomarker paleothermometry. *Climate of the Past*, *16*(5), 1667–1689. https://doi.org/10.5194/cp-16-1667-2020

Crouch, E., Shepherd, C., Morgans, H., Naafs, B., Dallanave, E., Phillips, A., et al. (2020). Climatic and environmental changes across the early Eocene climatic optimum at mid-Waipara River, Canterbury Basin, New Zealand. *Earth-Science Reviews*, *200*, 102961. https://doi.org/10.1016/j.earscirev.2019.102961

de Bar, M., de Nooijer, L., Schouten, S., Ziegler, M., Sluijs, A., & Reichart, G. J. (2019). Comparing seawater temperature proxy records for the past 90 Myrs from the shallow shelf record Bass River, New Jersey. *Paleoceanography and Paleoclimatology*, *34*(4), 455–475. https://doi.org/10.1029/2018pa003453

Evans, D. (2023). dbjevans/MgCaRB: V1.0 (v1.0) [Software]. Zenodo. https://doi.org/10.5281/zenodo.10200630

Evans, D., Sagoo, N., Renema, W., Cotton, L. J., Müller, W., Todd, J. A., et al. (2018). Eocene greenhouse climate revealed by coupled clumped isotope-Mg/Ca thermometry. *Proceedings of the National Academy of Sciences*, *115*(6), 1174–1179. https://doi.org/10.1073/pnas.1714744115

Fung, M. K., Katz, M. E., Miller, K. G., Browning, J. V., & Rosenthal, Y. (2019). Sequence stratigraphy, micropaleontology, and foraminiferal geochemistry, Bass River, New Jersey paleoshelf, USA: Implications for Eocene ice-volume changes. *Geosphere*, *15*(2), 502–532. https://doi.org/10.1130/ges01652.1

Gothmann, A. M., Stolarski, J., Adkins, J. F., Schoene, B., Dennis, K. J., Schrag, D. P., et al. (2015). Fossil corals as an archive of secular variations in seawater chemistry since the Mesozoic. *Geochimica et Cosmochimica Acta*, *160*, 188–208. https://doi.org/10.1016/j.gca.2015.03.018

Gray, W. R., & Evans, D. (2019). Nonthermal influences on Mg/Ca in planktonic foraminifera: A review of culture studies and application to the last glacial maximum. *Paleoceanography and Paleoclimatology*, *34*(3), 306–315. https://doi.org/10.1029/2018pa003517

Herold, N., Buzan, J., Seton, M., Goldner, A., Green, J., Müller, R., et al. (2014). A suite of early Eocene (~55 Ma) climate model boundary conditions: Geoscientific Model Development.

Hohbein, M. W., Sexton, P. F., & Cartwright, J. A. (2012). Onset of North Atlantic Deep Water production coincident with inception of the Cenozoic global cooling trend. *Geology*, *40*(3), 255–258. https://doi.org/10.1130/g32461.1

Hollis, C. J., Dunkley Jones, T., Anagnostou, E., Bijl, P. K., Cramwinckel, M. J., Cui, Y., et al. (2019). The DeepMIP contribution to PMIP4: Methodologies for selection, compilation and analysis of latest Paleocene and early Eocene climate proxy data, incorporating version 0.1 of the DeepMIP database. *Geoscientific Model Development*, *12*(7), 3149–3206. https://doi.org/10.5194/gmd-12-3149-2019

Hollis, C. J., Handley, L., Crouch, E. M., Morgans, H. E., Baker, J. A., Creech, J., et al. (2009). Tropical sea temperatures in the high-latitude South Pacific during the Eocene. *Geology*, *37*(2), 99–102. https://doi.org/10.1130/g25200a.1

Hollis, C. J., Taylor, K. W. R., Handley, L., Pancost, R. D., Huber, M., Creech, J. B., et al. (2012). Early Paleogene temperature history of the southwest Pacific Ocean: Reconciling proxies and models. *Earth and Planetary Science Letters*, *349–350*(0), 53–66. https://doi.org/10.1016/j.epsl.2012.06.024

Hopmans, E. C., Schouten, S., & Damsté, J. S. S. (2016). The effect of improved chromatography on GDGT-based palaeoproxies. *Organic Geochemistry*, *93*, 1–6. https://doi.org/10.1016/j.orggeochem.2015.12.006

Hutchinson, D. K., Coxall, H. K., O'Regan, M., Nilsson, J., Caballero, R., & de Boer, A. M. (2019). Arctic closure as a trigger for Atlantic overturning at the Eocene-Oligocene transition. *Nature Communications*, *10*(1), 3797. https://doi.org/10.1038/s41467-019-11828-z

Inglis, G. N. (2023). Surface ocean cooling in the Eocene North Atlantic coincides with declining atmospheric CO_2 [Dataset]. OSF. https://doi.org/10.17605/OSF.IO/BGTRU

Inglis, G. N., Farnsworth, A., Lunt, D., Foster, G. L., Hollis, C. J., Pagani, M., et al. (2015). Descent toward the icehouse; Eocene sea surface cooling inferred from GDGT distributions. *Paleoceanography*, *30*(7), 1000–1020. https://doi.org/10.1002/2014pa002723

Keating-Bitonti, C. R., Ivany, L. C., Affek, H. P., Douglas, P., & Samson, S. D. (2011). Warm, not super-hot, temperatures in the early Eocene subtropics. *Geology*, *39*(8), 771–774. https://doi.org/10.1130/g32054.1

Liu, Z., Pagani, M., Zinniker, D., DeConto, R., Huber, M., Brinkhuis, H., et al. (2009). Global cooling during the Eocene-Oligocene climate transition. *Science*, *323*(5918), 1187–1190. https://doi.org/10.1126/science.1166368

Liu, Z., He, Y., Jiang, Y., Wang, H., Liu, W., Bohaty, S. M., & Wilson, P. A. (2018). Transient temperature asymmetry between hemispheres in the Palaeogene Atlantic Ocean. *Nature Geoscience*, *11*(9), 656–660. https://doi.org/10.1038/s41561-018-0182-9

Lunt, D. J., Bragg, F., Chan, W.-L., Hutchinson, D. K., Ladant, J.-B., Morozova, P., et al. (2021). DeepMIP: Model intercomparison of early Eocene climatic optimum (EECO) large-scale climate features and comparison with proxy data. *Climate of the Past*, *17*(1), 203–227. https://doi.org/10.5194/cp-17-203-2021

Lunt, D. J., Huber, M., Anagnostou, E., Baatsen, M. L. J., Caballero, R., DeConto, R., et al. (2017). The DeepMIP contribution to PMIP4: Experimental design for model simulations of the EECO, PETM, and pre-PETM (version 1.0). *Geoscientific Model Development*, *10*(2), 889–901. https://doi.org/10.5194/gmd-10-889-2017

Miller, K. G., Browning, J. V., Sugarman, P. J., McLaughlin, P. P., Kominz, M. A., Olsson, R. K., et al. (2003). 174AX Leg summary: Sequences, sea level, tectonics, and aquifer resources: Coastal plain drilling. In K. G. Miller, P. J. Sugarman, & J. V. Browning (Eds.) *Proceedings of ocean drilling program, initial reports, 174AX (suppl.)* (pp. 1–40).

Miller, K. G., Sugarman, P. J., Browning, J. V., Olsson, R. K., Pekar, S. F., Reilly, T. J., et al. (1998). Bass River site. Proceedings of the ocean drilling program, initial reports, 174AX (pp. 5–43).

Müller, W., Shelley, M., Miller, P., & Broude, S. (2009). Initial performance metrics of a new custom-designed ArF excimer LA-ICPMS system coupled to a two-volume laser-ablation cell. *Journal of Analytical Atomic Spectrometry*, *24*(2), 209–214. https://doi.org/10.1039/b805995k

Norris, R., Klaus, A., & Kroon, D. (2001). Mid-Eocene deep water, the late Palaeocene thermal maximum and continental slope mass wasting during the Cretaceous-Palaeogene impact. *Geological Society, London, Special Publications*, *183*(1), 23–48. https://doi.org/10.1144/gsl.sp.2001.183.01.02

Pearson, P. N., van Dongen, B. E., Nicholas, C. J., Pancost, R. D., Schouten, S., Singano, J. M., & Wade, B. S. (2007). Stable warm tropical climate through the Eocene Epoch. *Geology*, *35*(3), 211–214. https://doi.org/10.1130/g23175a.1

Rae, J. W., Zhang, Y. G., Liu, X., Foster, G. L., Stoll, H. M., & Whiteford, R. D. (2021). Atmospheric CO_2 over the past 66 million years from marine archives. *Annual Review of Earth and Planetary Sciences*, *49*(1), 609–641. https://doi.org/10.1146/annurev-earth-082420-063026

Roberts, C. D., LeGrande, A. N., & Tripati, A. K. (2009). Climate sensitivity to Arctic seaway restriction during the early Paleogene. *Earth and Planetary Science Letters*, *286*(3–4), 576–585. https://doi.org/10.1016/j.epsl.2009.07.026

Shackleton, N. J., & Kennett, J. P. (1975). Paleotemperature history of the cenozoic and the initiation of Antarctic glaciation: Oxygen and carbon isotope analyses in DSDP sites 277, 279, and 281. *Initial Reports of the Deep Sea Drilling Project*, *29*, 743–755.

Sijp, W. P., England, M. H., & Huber, M. (2011). Effect of the deepening of the Tasman Gateway on the global ocean. *Paleoceanography*, *26*(4), 4207. https://doi.org/10.1029/2011pa002143

Sijp, W. P., von der Heydt, A. S., & Bijl, P. K. (2016). Model simulations of early westward flow across the Tasman Gateway during the early Eocene. *Climate of the Past*, *12*(4), 807–817. https://doi.org/10.5194/cp-12-807-2016

Straume, E. O., Nummelin, A., Gaina, C., & Nisancioglu, K. H. (2022). Climate transition at the Eocene–Oligocene influenced by bathymetric changes to the Atlantic–Arctic oceanic gateways. *Proceedings of the National Academy of Sciences*, *119*(17), e2115346119. https://doi.org/10.1073/pnas.2115346119

Tierney, J. E., & Tingley, M. P. (2014). A Bayesian, spatially-varying calibration model for the TEX_{86} proxy. *Geochimica et Cosmochimica Acta*, *127*, 83–106. https://doi.org/10.1016/j.gca.2013.11.026

Thornalley, D. J., Elderfield, H., & McCave, I. N. (2011). Reconstructing North Atlantic deglacial surface hydrography and its link to the Atlantic overturning circulation. *Global and Planetary Change*, *79*(3–4), 163–175. https://doi.org/10.1016/j.gloplacha.2010.06.003

Vahlenkamp, M., Niezgodzki, I., De Vleeschouwer, D., Lohmann, G., Bickert, T., & Pälike, H. (2018). Ocean and climate response to North Atlantic seaway changes at the onset of long-term Eocene cooling. *Earth and Planetary Science Letters*, *498*, 185–195. https://doi.org/10.1016/j.epsl.2018.06.031

Vandenberghe, N., Hilgen, F. J., & Speijer, R. P. (2012). The Paleogene period. In F. Gradstein, J. Ogg, M. Schmitz, & G. Ogg (Eds.), *The geological time scale 2012* (pp. 855–921). Elsevier.

Van Der Ploeg, R., Cramwinckel, M. J., Kocken, I. J., Leutert, T. J., Bohaty, S. M., Fokkema, C. D., et al. (2023). North Atlantic surface ocean warming and salinization in response to middle Eocene greenhouse warming. *Science Advances*, *9*(4), eabq0110. https://doi.org/10.1126/sciadv.abq0110

Westerhold, T., Marwan, N., Drury, A. J., Liebrand, D., Agnini, C., Anagnostou, E., et al. (2020). An astronomically dated record of Earth's climate and its predictability over the last 66 million years. *Science*, *369*(6509), 1383–1387. https://doi.org/10.1126/science.aba6853

Witkowski, J., Bryłka, K., Bohaty, S. M., Mydłowska, E., Penman, D. E., & Wade, B. S. (2021). North Atlantic marine biogenic silica accumulation through the early to middle Paleogene: Implications for ocean circulation and silicate weathering feedback. *Climate of the Past*, *17*(5), 1937–1954. https://doi.org/10.5194/cp-17-1937-2021

Zachos, J., Pagani, M., Sloan, L., Thomas, E., & Billups, K. (2001). Trends, rhythms, and aberrations in global climate 65 Ma to present. *Science*, *292*(5517), 686–693. https://doi.org/10.1126/science.1059412

Zhang, Y., de Boer, A. M., Lunt, D. J., Hutchinson, D. K., Ross, P., van de Flierdt, T., et al. (2022). Early Eocene ocean meridional overturning circulation: The roles of atmospheric forcing and strait geometry. *Paleoceanography and Paleoclimatology*, *37*(3), e2021PA004329. https://doi.org/10.1029/2021pa004329

Zhang, Y. G., Pagani, M., Liu, Z., Bohaty, S. M., & DeConto, R. (2013). A 40-million-year history of atmospheric CO_2. *Philosophical Transactions of the Royal Society A: Mathematical, Physical & Engineering Sciences*, *371*(2001), 20130096. https://doi.org/10.1098/rsta.2013.0096

Zhang, Z., Nisancioglu, K. H., Flatøy, F., Bentsen, M., Bethke, I., & Wang, H. (2011). Tropical seaways played a more important role than high latitude seaways in Cenozoic cooling. *Climate of the Past*, *7*(3), 801–813. https://doi.org/10.5194/cp-7-801-2011

Zhu, J., Poulsen, C. J., Otto-Bliesner, B. L., Liu, Z., Brady, E. C., & Noone, D. C. (2020). Simulation of early Eocene water isotopes using an Earth system model and its implication for past climate reconstruction. *Earth and Planetary Science Letters*, *537*, 116164. https://doi.org/10.1016/j.epsl.2020.116164

Zhu, J., Poulsen, C. J., & Tierney, J. E. (2019). Simulation of Eocene extreme warmth and high climate sensitivity through cloud feedbacks. *Science Advances*, *5*(9), eaax1874. https://doi.org/10.1126/sciadv.aax1874

References From the Supporting Information

Barker, S., Cacho, I., Benway, H., & Tachikawa, K. (2005). Planktonic foraminiferal Mg/Ca as a proxy for past oceanic temperatures: A methodological overview and data compilation for the last glacial maximum. *Quaternary Science Reviews*, *24*(7–9), 821–834. https://doi.org/10.1016/j.quascirev.2004.07.016

Evans, D., Brierley, C., Raymo, M. E., Erez, J., & Müller, W. (2016). Planktic foraminifera shell chemistry response to seawater chemistry: Pliocene–Pleistocene seawater Mg/Ca, temperature and sea level change. *Earth and Planetary Science Letters*, *438*, 139–148. https://doi.org/10.1016/j.epsl.2016.01.013

Evans, D., Bhatia, R., Stoll, H., & Müller, W. (2015). LA-ICPMS Ba/Ca analyses of planktic foraminifera from the B ay of B engal: Implications for late P leistocene orbital control on monsoon freshwater flux. *Geochemistry, Geophysics, Geosystems*, *16*(8), 2598–2618. https://doi.org/10.1002/2015gc005822

Evans, D., Erez, J., Oron, S., & Müller, W. (2015). Mg/Ca-temperature and seawater-test chemistry relationships in the shallow-dwelling large benthic foraminifera Operculina ammonoides. *Geochimica et Cosmochimica Acta*, *148*, 325–342. https://doi.org/10.1016/j.gca.2014.09.039

Evans, D., & Müller, W. (2012). Deep time foraminifera Mg/Ca paleothermometry: Nonlinear correction for secular change in seawater Mg/Ca. *Paleoceanography*, *27*(4), PA4205. https://doi.org/10.1029/2012PA002315

Evans, D., & Müller, W. (2018). Automated extraction of a five-year LA-ICP-MS trace element data set of ten common glass and carbonate reference materials: Long-term data quality, optimisation and laser cell homogeneity. *Geostandards and Geoanalytical Research*, *42*(2), 159–188. https://doi.org/10.1111/ggr.12204

Holland, K., Branson, O., Haynes, L. L., Hönisch, B., Allen, K. A., Russell, A. D., et al. (2020). Constraining multiple controls on planktic foraminifera Mg/Ca. *Geochimica et Cosmochimica Acta*, *273*, 116–136. https://doi.org/10.1016/j.gca.2020.01.015

Hönisch, B., Allen, K. A., Lea, D. W., Spero, H. J., Eggins, S. M., Arbuszewski, J., et al. (2013). The influence of salinity on Mg/Ca in planktic foraminifers—Evidence from cultures, core-top sediments and complementary $\delta^{18}O$. *Geochimica et Cosmochimica Acta*, *121*, 196–213. https://doi.org/10.1016/j.gca.2013.07.028

Hopmans, E. C., Weijers, J. W., Schefuß, E., Herfort, L., Damsté, J. S. S., & Schouten, S. (2004). A novel proxy for terrestrial organic matter in sediments based on branched and isoprenoid tetraether lipids. *Earth and Planetary Science Letters*, *224*(1–2), 107–116. https://doi.org/10.1016/j.epsl.2004.05.012

Jochum, K. P., Stoll, B., Herwig, K., Willbold, M., Hofmann, A. W., Amini, M., et al. (2006). MPI-DING reference glasses for in situ microanalysis: New reference values for element concentrations and isotope ratios. *Geochemistry, Geophysics, Geosystems*, *7*(2), 1525. https://doi.org/10.1029/2005gc001060

Kim, J. H., Van der Meer, J., Schouten, S., Helmke, P., Willmott, V., Sangiorgi, F., et al. (2010). New indices and calibrations derived from the distribution of crenarchaeal isoprenoid tetraether lipids: Implications for past sea surface temperature reconstructions. *Geochimica et Cosmochimica Acta*, *74*(16), 4639–4654. https://doi.org/10.1016/j.gca.2010.05.027

Longerich, H. P., Jackson, S. E., & Günther, D. (1996). Inter-laboratory note. Laser ablation inductively coupled plasma mass spectrometric transient signal data acquisition and analyte concentration calculation. *Journal of Analytical Atomic Spectrometry*, *11*(9), 899–904. https://doi.org/10.1039/ja9961100899

Miller, K. G., Kominz, M. A., Browning, J. V., Wright, J. D., Mountain, G. S., Katz, M. E., et al. (2005). The Phanerozoic record of global sea-level change. *Science*, *310*(5752), 1293–1298. https://doi.org/10.1126/science.1116412

Miller, K. G., Sugarman, P. J., Browning, J. V., Kominz, M. A., Hernández, J. C., Olsson, R. K., et al. (2003). Late Cretaceous chronology of large, rapid sea-level changes: Glacioeustasy during the greenhouse world. *Geology*, *31*(7), 585–588. https://doi.org/10.1130/0091-7613(2003)031<0585:lccolr>2.0.co;2

Mucci, A., & Morse, J. W. (1983). The incorporation of Mg^{2+} and Sr^{2+} into calcite overgrowths: Influences of growth rate and solution composition. *Geochimica et Cosmochimica Acta*, *47*(2), 217–233. https://doi.org/10.1016/0016-7037(83)90135-7

Pearson, P. N., Olsson, R. K., Huber, B. T., Hemleben, C., & Berggren, W. A. (2006). *Atlas of Eocene planktonic foraminifera*. Cushman Foundation for Foraminiferal Research. Special Publication (No. 41).

Rattanasriampaipong, R., Zhang, Y. G., Pearson, A., Hedlund, B. P., & Zhang, S. (2022). Archaeal lipids trace ecology and evolution of marine ammonia-oxidizing archaea. *Proceedings of the National Academy of Sciences*, *119*(31), e2123193119. https://doi.org/10.1073/pnas.2123193119

Spratt, R. M., & Lisiecki, L. E. (2016). A Late Pleistocene sea level stack. *Climate of the Past*, *12*(4), 1079–1092. https://doi.org/10.5194/cp-12-1079-2016

Taylor, K. W., Huber, M., Hollis, C. J., Hernandez-Sanchez, M. T., & Pancost, R. D. (2013). Re-evaluating modern and Palaeogene GDGT distributions: Implications for SST reconstructions. *Global and Planetary Change*, *108*, 158–174. https://doi.org/10.1016/j.gloplacha.2013.06.011

Wit, J. C., Reichart, G.-J., A Jung, S. J., & Kroon, D. (2010). Approaches to unravel seasonality in sea surface temperatures using paired single-specimen foraminiferal $d^{18}O$ and Mg/Ca analyses. *Paleoceanography*, *25*(4), PA4220. https://doi.org/10.1029/2009PA001857

Zeebe, R. E., & Tyrrell, T. (2019). History of carbonate ion concentration over the last 100 million years II: Revised calculations and new data. *Geochimica et Cosmochimica Acta*, *257*, 373–392. https://doi.org/10.1016/j.gca.2019.02.041

Zhang, Y. G., Zhang, C. L., Liu, X. L., Li, L., Hinrichs, K. U., & Noakes, J. E. (2011). Methane index: A tetraether archaeal lipid biomarker indicator for detecting the instability of marine gas hydrates. *Earth and Planetary Science Letters*, *307*(3–4), 525–534. https://doi.org/10.1016/j.epsl.2011.05.031